

# DNS OF PASSIVE SCALAR TRANSPORT FIELDS IN TURBULENT FLOW AT LOW AND HIGH PRANDTL NUMBERS

*B. Chaouat*

*ONERA, 92322 Châtillon, France*

**Bruno.Chaouat@onera.fr**

## Abstract

We perform several DNS of the turbulent channel flow including a passive scalar with different boundary conditions at the Reynolds number  $R_\tau = 395$  and the Prandtl numbers  $P_r = 0.01, 0.1, 1$  and  $10$ . The case I is a plane channel flow heated on both walls whereas the case II is a plane channel heated only from one wall but cooled from the other one at the same rate. In addition, different boundary conditions are applied for the passive scalar at the wall. For the case I, the iso-scalar boundary condition  $\theta_w = 0$  is imposed at the wall implying that its fluctuation is zero whereas for the case II,  $\theta_w$  is not prescribed to a fixed value so that it is fluctuating in time at the wall. For both cases, the distributions of the mean scalar field, root-mean-square fluctuation, turbulent heat flux, turbulent Prandtl number are examined in detail. Moreover, some insights of the flow structure of the scalar fields are provided. As a result, the conduction region penetrates less deeply into the core region of the channel as the Prandtl number increases from  $0.01$  to  $10$ . Owing to the different boundary conditions applied at the wall for both cases, significant differences in the evolution of the scalar field are observed in the channel. The impacts of the wall scalar fluctuations on the scalar field are appreciable within the near-wall region.

## 1 Introduction

Turbulent flows involving the transport of passive scalar are encountered in many engineering applications in industrial plants but also in nature like for instance the pollution dispersal in atmosphere. In the case of small variation of the scalar field, the turbulent velocity field governs the scalar field while the influence of the scalar field on the velocity field can be neglected in a first approximation. Direct numerical simulation (DNS) solving all the turbulence and thermal scales is the best tool to investigate turbulent scalar fields and allows also to validate closure models with heat transfer used in Reynolds averaged Navier-Stokes (RANS) modeling (Hanjalic and Launder, 2011; Matsubara et al., 2012), large eddy simulation (LES) and hybrid RANS/LES modeling (Chaouat, 2017; Kenjeres and Hanjalic, 2006).

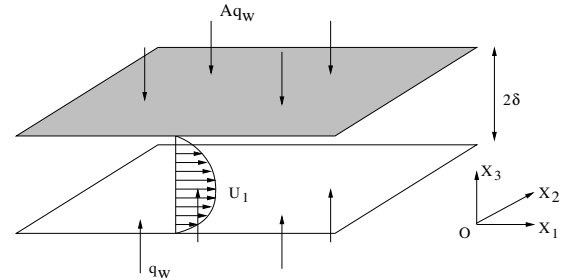


Figure 1: Setup of the numerical channel flow simulations with various thermal boundary conditions. wall heated ( $A=1$ ); wall cooled ( $A=-1$ ).

We consider the turbulent heat transfer in a plane channel heated on both walls with a constant time-averaged heat flux (case I) and a channel heated with a constant heat flux only from one wall but cooled from the other one at the same rate (case II) as shown in Figure 1. The case I has been studied by several authors such as Kawamura et al. (1999) at  $R_\tau = u_\tau \delta / \nu = 150, 180, 395$  based on the friction velocity  $u_\tau$ , the channel half width  $\delta$  and the molecular viscosity, with the Prandtl number  $P_r = 0.025, 0.2, 0.71$ ; Kozuka et al., (2009) at  $R_\tau = 180, 395$  with  $P_r = 0.71, 1, 2, 7, 10$ . Physically, these Prandtl numbers are associated with heat transfer of a liquid metal such as mercury ( $P_r \approx 0.015$ ), gases ( $P_r \approx 1$ ), water ( $P_r \approx 5 - 7$ ), and seawater ( $P_r \approx 13$  at  $0^\circ C$ ) depending on the temperature. Simulations of the plane channel flow heated on both walls (case I) allowed to obtain the mean field parameters as well as the thermal turbulence statistics such as the variance of temperature fluctuation  $k_\theta = \langle \theta' \theta' \rangle / 2$ , the turbulent heat fluxes and the turbulent Prandtl number  $P_{rt}$ . The budgets of transport equations for the variance of temperature  $k_\theta$  (Kawamura et al., 1999), the dissipation-rate  $\epsilon_\theta$  and turbulent heat fluxes (Kawamura et al., 2009) were also investigated in detail thanks to high grid resolutions. If this case was performed in the past by several authors, the results are scattered across several papers so that an overview is desirable to cover the range of the Prandtl number varying from low to high values. On the contrary, the case II was only treated by Lyon et al. (1991) at the low Reynolds number  $R_\tau = 150$  and Prandtl

number  $P_r = 1$  considering however a constant wall temperature. The case including fluctuation in time of the scalar  $\theta$  at the wall was not previously studied so that new results are here presented for the first time.

In this work, we perform direct numerical simulations of the fully turbulent channel flow corresponding to cases I and II with different boundary conditions at the Reynolds number  $R_\tau = 395$  and the Prandtl numbers  $P_r = 0.01, 0.1, 1, 10$ . The passive scalar is here interpreted as the temperature in heat transfer but more generally as any variable involving a passive contaminant associated with mass transfer. The objective is to compare both the mean and *rms* scalar fields associated with these two cases and to investigate the impacts of the wall passive scalar fluctuation on the scalar field.

## 2 Equations, boundary conditions and numerical procedure

The momentum equation reads

$$\frac{\partial u_i^+}{\partial t^+} + \frac{\partial}{\partial x_j^+} (u_i^+ u_j^+) = -\frac{\partial p^+}{\partial x_i^+} + \frac{1}{R_\tau} \frac{\partial^2 u_i^+}{\partial x_j^+ \partial x_j^+} + G_i \quad (1)$$

where in this equation,  $u_i$  and  $p$  denote the velocity and pressure, respectively, the coordinate and flow variables are normalized by the channel half width  $\delta$ , the friction velocity  $u_\tau$ , the kinematic viscosity  $\nu$ . The quantity  $G_i = \delta_{1i}$  denotes the source term that has the effect to balance the friction at the upper and lower walls to get periodic condition between the inlet and outlet sections of the channel. The transport equation for the passive scalar  $\theta$  reads

$$\frac{\partial \theta^+}{\partial t^+} + \frac{\partial}{\partial x_j^+} (\theta^+ u_j^+) = \frac{1}{R_\tau P_r} \frac{\partial^2 \theta^+}{\partial x_j^+ \partial x_j^+} + Q \quad (2)$$

where in this equation,  $Q$  denotes the source term. Its physical meaning corresponds to the mean temperature gradient necessary to balance wall heat fluxes. The variable  $\theta$  is normalized by the surface scalar flux defined as  $\theta_\tau = q_w / (\rho c_p u_\tau)$  where  $\rho$ ,  $c_p$  and  $q_w$  are the fluid density, the specific heat at constant pressure and the heat flux at the wall. The heat flux is given by  $q_w = -\kappa (\partial \theta / \partial x_3)_w$  where  $\kappa$  stands for the thermal conductivity  $\kappa = \rho c_p \nu / P_r$ . The thermal diffusivity is given by  $\sigma = \kappa / (\rho c_p) = \nu / P_r$ . Two different boundary conditions are used for the scalar field according to the parameter  $A$  (see Fig 1). In case I,  $A = 1$ , where both walls are heated,  $Q = -u_1^+ / U_b^+$  to ensure zero mean gradient of the passive scalar  $\partial \langle \theta \rangle / \partial x_1 = 0$ , whereas in case II,  $A = -1$ ,  $Q = 0$ , i.e., an internal heat source is not required to get a fully developed thermally flow.

### Boundary conditions

For both cases, the boundary conditions at the walls  $x_3 = 0$  and  $2\delta$  are no slip velocity  $u_i^+ = 0$

and constant heat flux, i.e., isoflux boundary condition ( $H_1$ ). For the case I, the isoscalar boundary condition ( $H_2$ ) is also imposed at the wall leading to  $\theta_w = 0$  whereas for the case II,  $\theta_w$  is not prescribed to a fixed value so that it is fluctuating in time at the wall (Lu, D.M, Hetsroni, G., 1995). This choice is motivated to account for the two extreme thermal conditions that can be encountered in engineering applications or experimental facilities (Mosyak et al., 2001). Indeed, as mentioned by Kasagi et al., (1989), it is not straightforward to give the thermal boundary condition on the wall which is in contact with the turbulent flow because of the unsteady heat conduction in the solid associated with the unsteadiness of turbulence.

### Numerical procedure

The dimension of the channel in the streamwise, spanwise and normal directions along the axes  $x_1, x_2, x_3$  are  $L_1 = 6.4\delta$ ,  $L_2 = 3.2\delta$  and  $L_3 = 2\delta$ . The number of grid points is determined with the aim to solve both the Kolmogorov scale  $\eta_\kappa = (\nu^3/\epsilon)^{1/4}$  and the Batchelor length-scale  $\eta_\theta$  (Batchelor, 1959; Tennekes and Lumley, 1972) which approaches  $\eta_\kappa$  at  $P_r$  of order of unity  $\eta_\theta \approx \eta_\kappa$ , but  $\eta_\theta = (\sigma^3/\epsilon)^{1/4} = \eta_\kappa / P_r^{3/4}$  at small Prandtl numbers and  $\eta_\theta = (\nu\sigma^2/\epsilon)^{1/4} = \eta_\kappa / P_r^{1/2}$  at large Prandtl numbers. At  $P_r = 0.01$ ,  $\eta_\theta \approx 31.6 \eta_\kappa$ , at  $P_r = 0.1$ ,  $\eta_\theta \approx 5.62 \eta_\kappa$ , at  $P_r = 1$ ,  $\eta_\theta \approx \eta_\kappa$  but at  $P_r = 10$ ,  $\eta_\theta \approx 0.316 \eta_\kappa$ . For the Reynolds and Prandtl number values studied here, the grid numbers vary from the mesh  $M_1$  of resolution  $256 \times 128 \times 256$  for  $P_r = 0.01$  and  $0.1$  to  $M_2$  of resolution  $512 \times 256 \times 256$  for  $P_r = 1$  and  $M_3$  of resolution  $1024 \times 512 \times 512$  for  $P_r = 10$ . For all meshes, the spacings are  $\Delta_1^+ = \Delta_2^+ \approx 10$  for  $M_1$ ,  $\Delta_1^+ = \Delta_2^+ \approx 5$  for  $M_2$  and  $\Delta_1^+ = \Delta_2^+ \approx 2.5$  for  $M_3$ . The equations are integrated in time using an explicit Runge-Kutta scheme of fourth order accuracy in time and solved in space by means of a centered scheme of fourth order accuracy in space. The CFD code (Chaouat, 2011) is based on the finite volume technique and is optimized with message passing interface (MPI).

## 3 Turbulent channel flow heated on both walls (case I)

The transformed variable  $\Theta^+ = \theta_w^+ - \theta^+$  is considered to analyze the present results. Figs. 2 and 3 show the mean scalar variable  $\Theta^+$  and its *rms* versus the logarithmic and linear wall distance, respectively. The logarithmic region of the mean scalar is well visible at  $R_\tau = 395$ . Overall, these results compare very well with previous simulations (Kawamura et al., 1998-1999; Kozuga et al. 2009) although the Reynolds number and Prandtl numbers may take on different values. As a result, when the Prandtl number increases from 0.01 to 10, the thermal effect is more pronounced. The conduction region penetrates less deeply into the core region of the channel, the *rms* scalar variance  $\theta_{rms}$  is of higher order magnitude, and

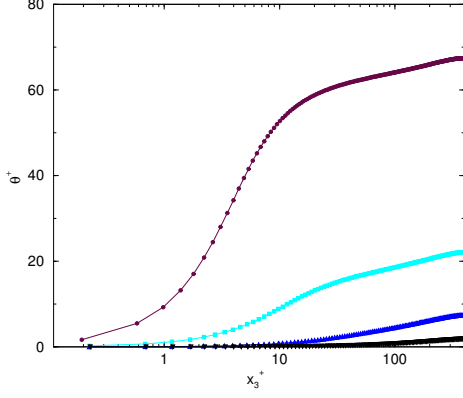


Figure 2: Mean scalar field at different Prandtl numbers in logarithmic coordinate.  $P_r = 0.01$ ,  $\blacktriangledown$ .  $P_r = 0.1$ ,  $\blacktriangle$ .  $P_r = 1$ ,  $\blacktriangle$ .  $P_r = 10$ ,  $\blacksquare$ .  $R_\tau = 395$ ,  $\bullet$ .

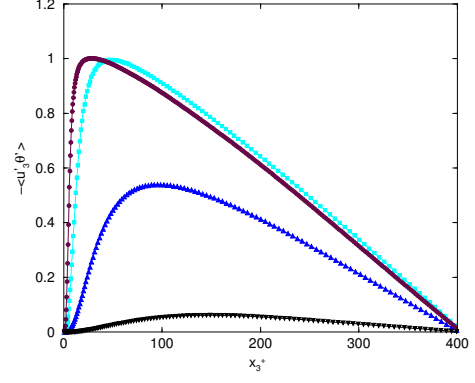


Figure 4: Normal turbulent heat flux  $q_3 = -\langle u_3^+ \theta'^+ \rangle$  versus the wall coordinate.  $P_r = 0.01$ ,  $\blacktriangledown$ .  $P_r = 0.1$ ,  $\blacktriangle$ .  $P_r = 1$ ,  $\blacktriangle$ .  $P_r = 10$ ,  $\blacksquare$ .  $R_\tau = 395$ ,  $\bullet$ .

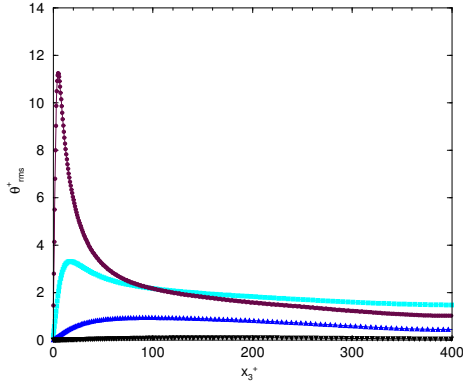


Figure 3: Root mean square of the scalar variance versus the wall unit.  $P_r = 0.01$ ,  $\blacktriangledown$ .  $P_r = 0.1$ ,  $\blacktriangle$ .  $P_r = 1$ ,  $\blacktriangle$ .  $P_r = 10$ ,  $\blacksquare$ .  $R_\tau = 395$ ,  $\bullet$ .

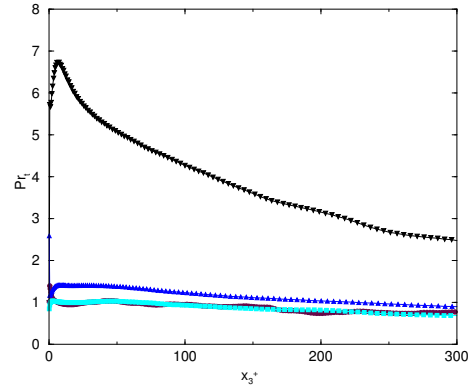


Figure 5: Profiles of the turbulent Prandtl number versus the wall unit.  $P_r = 0.01$ ,  $\blacktriangledown$ .  $P_r = 0.1$ ,  $\blacktriangle$ .  $P_r = 1$ ,  $\blacktriangle$ .  $P_r = 10$ ,  $\blacksquare$ .  $R_\tau = 395$ ,  $\bullet$ .

the peak values location moves close to the walls. Fig. 4 shows the profile of the normal turbulent heat flux  $q_3^+ = -\langle u_3^+ \theta'^+ \rangle$  versus the wall coordinate of the channel for all Prandtl numbers. As the Prandtl number increases, the normal turbulent heat flux becomes larger and the peak value moves to the wall. We now examine the validity of the gradient law hypothesis of the turbulent heat flux modeling. The Prandtl number is defined itself as the ratio of the turbulent eddy viscosity  $\nu_t$  to the turbulent eddy diffusivity  $\sigma_t$

$$Pr_t = \frac{\langle u_1' u_3' \rangle \partial \langle \theta \rangle / \partial x_3}{\langle \theta' u_3' \rangle \partial \langle u_1 \rangle / \partial x_3} \quad (3)$$

Fig. 5 exhibits the profile of the turbulent Prandtl number versus the wall unit. At the Prandtl numbers  $P_r = 0.1$ , 1 and 10, one can see that the turbulent Prandtl number reaches an asymptotic behavior independent of the molecular Prandtl number, except however in the near wall region where a very small variation of a few percent is observed. Away from the wall, the turbulent Prandtl number approaches unity. This outcome confirms the hypothesis of a constant turbu-

lent Prandtl number at moderate and high molecular Prandtl numbers. But at the very low value  $P_r = 0.01$ , the turbulent Prandtl number varies strongly with respect to the wall-normal coordinate. It increases significantly from the value 6 to 7 in the immediate vicinity of the wall and then gradually decreases when approaching the center of the channel.

#### 4 Turbulent channel flow heated on one wall and cooled on the other one (case II)

The transformed variable  $\Theta^+ = 2\theta^+ / (\theta_{w1}^+ - \theta_{w2}^+)$  is chosen because of the thermal configuration of this case. Figs. 6 and 7 show the mean scalar variable  $\Theta^+$  and its *rms* versus the wall distance, respectively. As expected, the mean scalar profiles are antisymmetric about the channel centerline with non-zero gradients at the center. The mean profiles are steeper as the Prandtl number increases from 0.01 to 10 resulting from the effects of the thermal diffusivity at small Prandtl number and by the momentum diffusivity at large Prandtl number. As for the case I, the magnitude of the scalar variance is higher at large Prandtl num-

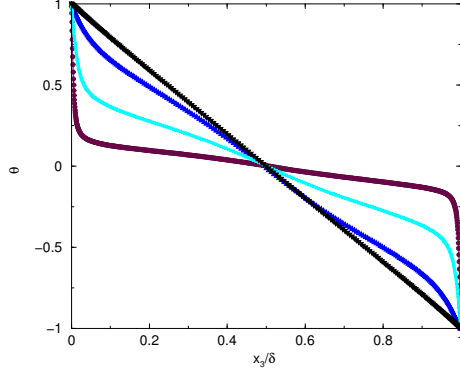


Figure 6: Mean scalar field at different Prandtl numbers in wall coordinate.  $P_r = 0.01$ ,  $\blacktriangledown$ .  $P_r = 0.1$ ,  $\blacktriangle$ .  $P_r = 1$ ,  $\blacktriangle$ .  $P_r = 10$ ,  $\blacksquare$ .  $R_\tau = 395$ .

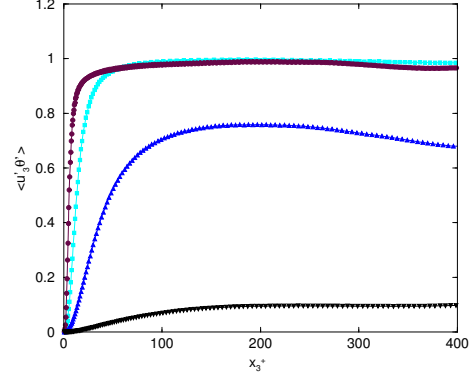


Figure 8: Normal turbulent heat flux  $|q_3| = \langle u_3' \theta'^+ \rangle$  versus the wall coordinate.  $P_r = 0.01$ ,  $\blacktriangledown$ .  $P_r = 0.1$ ,  $\blacktriangle$ .  $P_r = 1$ ,  $\blacktriangle$ .  $P_r = 10$ ,  $\blacksquare$ .  $R_\tau = 395$ .

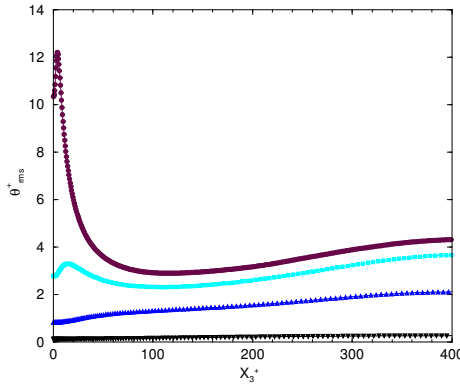


Figure 7: Root mean square of the scalar variance versus the wall unit.  $P_r = 0.01$ ,  $\blacktriangledown$ .  $P_r = 0.1$ ,  $\blacktriangle$ .  $P_r = 1$ ,  $\blacktriangle$ .  $P_r = 10$ ,  $\blacksquare$ .  $R_\tau = 395$ .

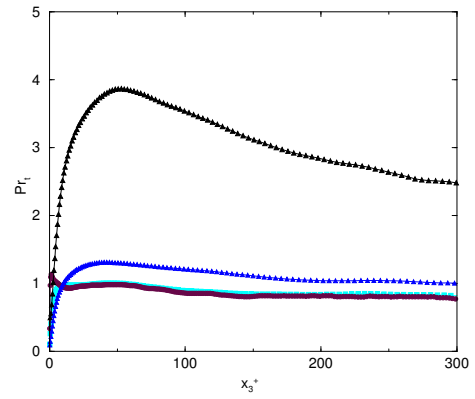


Figure 9: Profiles of the turbulent Prandtl number versus the wall unit.  $P_r = 0.01$ ,  $\blacktriangledown$ .  $P_r = 0.1$ ,  $\blacktriangle$ .  $P_r = 1$ ,  $\blacktriangle$ .  $P_r = 10$ ,  $\blacksquare$ .  $R_\tau = 395$ .

bers than at low  $P_r$  but in the contrary to the case I, it is not reduced to zero in the near wall-region due to the boundary condition applied at the wall. Fig. 8 shows the profile of the normal turbulent heat flux versus the wall coordinate of the channel. In comparison with Fig. 4, the behavior of the normal heat fluxes associated with cases I and II are similar in the near wall region but quite different when moving away from the wall toward the center of the channel due to the distinct profiles of the mean passive scalar  $\theta$  as depicted in Figs 2 and 6. Indeed, in case I, the correlation  $\langle u_3' \theta' \rangle$  changes of sign when moving from the lower to the upper walls of the channel ( $u_3' > 0$ ,  $\theta' > 0$  for  $x_3 < \delta$  and  $u_3' < 0$ ,  $\theta' > 0$  for  $x_3 > \delta$ ) with  $\langle u_3' \theta' \rangle \approx 0$  at  $x_3 = \delta$  leading to an anti-symmetric profile while in case II, this correlation  $\langle u_3' \theta' \rangle$  remains always positive since both  $u_3'$  and  $\theta'$  change of sign ( $u_3' > 0$ ,  $\theta' > 0$  for  $x_3 < \delta$  and  $u_3' < 0$ ,  $\theta' < 0$  for  $x_3 > \delta$ ) leading to a symmetric profile. Fig. 9 exhibits the profile of the turbulent Prandtl number at  $P_r = 0.01, 0.1, 1$  and  $10$  versus the wall unit coordinate. As for the case I, the turbulent Prandtl number is almost constant except at the Prandtl number  $P_r = 0.01$ . The maximum value at

$P_r = 0.01$  is about 4 that is lower than the one reached in case I. But surprisingly, although the thermal configuration between cases I and II is different, the profile of the turbulent Prandtl number remains roughly the same whatever the fluctuation value  $\theta'$  at the wall. This outcome is of interest because these two cases are generic to many industrial applications involving heat transfer and reveals that the assumption of a constant turbulent Prandtl number still holds at moderate and high molecular Prandtl numbers regardless of the thermal configuration considered (heated or cooled wall) even if the instantaneous temperature is fluctuating in time at the wall.

## 5 Effect of the thermal boundary condition at the wall on the *rms* fluctuation

Although the thermal configuration of cases I and II is different leading to a symmetric or anti-symmetric profiles of the mean scalar field, some elements of comparison regarding the effect of the boundary condition of the scalar fluctuation at the wall are possible to put in light. More details are provided by plotting

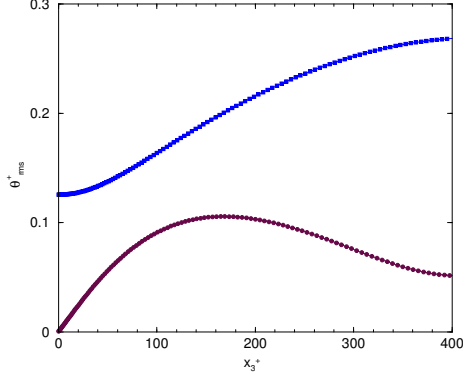


Figure 10: Root mean square of the scalar variance versus the wall unit at  $P_r = 0.01$ . Case I ●. Case II ■.

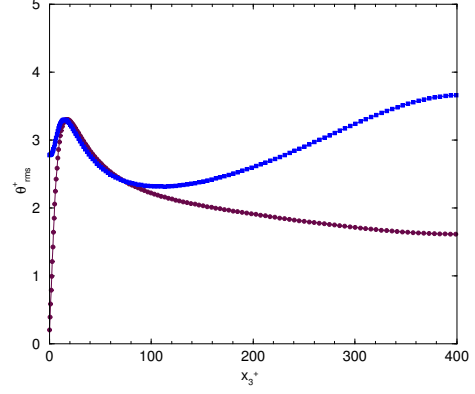


Figure 12: Root mean square of the scalar variance versus the wall unit at  $P_r = 1$ . Case I ●. Case II ■.

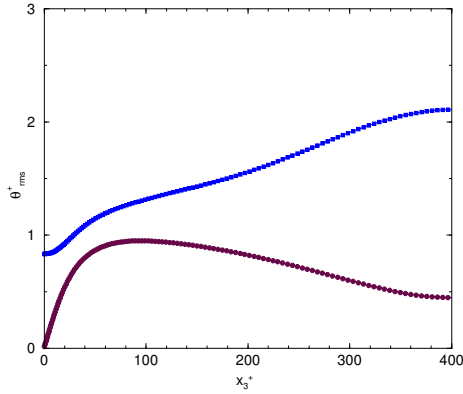


Figure 11: Root mean square of the scalar variance versus the wall unit at  $P_r = 0.1$ . Case I ●. Case II ■.

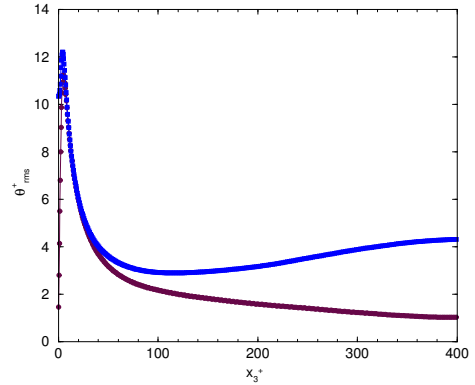


Figure 13: Root mean square of the scalar variance versus the wall unit at  $P_r = 10$ . Case I ●. Case II ■.

the *rms* profile at each Prandtl number associated with cases I and II, see Figs. 10 to 13. As the normal wall distance increases, the *rms* fluctuation associated with the case I begins to increase from zero to its maximum value in the vicinity of the wall, and then gradually decreases when going to the central region of the channel. By contrast, different situations occur for the case II depending on the Prandtl number value. For the Prandtl numbers  $P_r = 0.01$  and  $0.1$ , the *rms* fluctuation associated with case II slowly increases until reaching the central region of the channel whereas for  $P_r = 1$  and  $10$ , it rapidly increases and decreases showing a peak of intensity, and then gradually increases again when approaching the centerline. As a result, whatever the Prandtl number values, the difference between these two *rms* fluctuation associated with cases I and II remains significant in the center of the channel. One can invoke two reasons. Firstly, the turbulence activity caused by the fluctuation at the wall is sufficiently high to sustain when going away from the wall. Secondly, the production rate of the scalar variance  $P_\theta \approx -\langle u_3' \theta' \rangle \partial \langle \theta \rangle / \partial x_3$  is acting everywhere in the flow even in the center of the channel. That being said, in the near wall re-

gion, at the lower Prandtl numbers  $P_r = 0.01$  and  $0.1$ , the level of the scalar variance for the case I remains lower than the one obtained for the case II whereas at the Prandtl numbers  $P_r = 1$  and  $10$ , surprisingly, this level is roughly the same. In particular, the profiles of the scalar variance collapse with each other in the wall region since the peaks of the  $\theta_{rms}$  fluctuation match with one another at  $P_r = 1$  and  $10$ . But these profiles differ however from each other when going away from the wall for the reasons given above.

## 6 Structure of the scalar fields

For sake of conciseness, only the flow field associated with the case I is investigated. Fig. 14 displays the contours of the instantaneous scalar field  $\theta$  in the  $(x_1, x_3)$  mid-plane for the Prandtl numbers  $P_r = 0.01, 0.1, 1$  and  $10$ . As expected, according to the scale evolution of the Batchelor length-scale  $\eta_\theta$  with the Prandtl number, it appears that the structures get thinner as  $P_r$  is increasing. Moreover, these structures are less and less organized as the Prandtl numbers increase giving rise to the detachment of vortex substantially in the normal direction to the wall. A

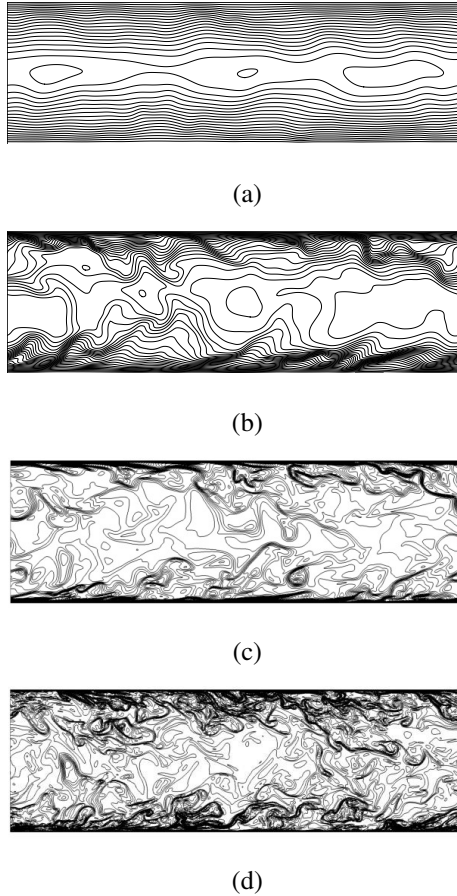


Figure 14: Contours of the instantaneous scalar field  $\Theta$  in the  $(x_1, x_3)$  mid-plane. (a)  $P_r = 0.01$ ; (b)  $P_r = 0.1$ ; (c)  $P_r = 1$ ; (d)  $P_r = 10$ ;  $R_\tau = 395$ .

strong activity of the passive scalar is observed in the near wall region corresponding to the peak of  $\theta_{rms}$  fluctuation as already highlighted in Fig. 3.

## 7 Conclusion

The DNS of turbulent channel flow with scalar transport has been performed at  $R_\tau = 395$  and at the Prandtl numbers  $P_r = 0.01, 0.1, 1$  and  $10$  with different flux conditions and boundary conditions of the passive scalar at the wall. As a result, the distributions of the mean scalar field, root mean square fluctuation, turbulent heat flux and turbulent Prandtl number were accurately obtained and the effect of the Prandtl number was investigated for both cases I and II. It has been demonstrated that the impacts of the wall passive scalar fluctuation on the scalar field are appreciable within the near wall region especially at low Prandtl numbers but tend however to diminish at moderate and high Prandtl numbers. In particular, except in the immediate vicinity of the wall, the profiles of the scalar variance collapse with each other in the wall region independently from the intensity of the wall passive scalar fluctuation at  $P_r = 1$  and  $10$ .

Moreover, the structure of the scalar fields was also examined showing that the structures get thinner as  $P_r$  is increasing. Further work will include the validation of hybrid RANS/LES models (Chaouat, 2017) such as PITM (Chaouat and Schiestel, 2005) in presence of passive scalar transport fields.

## References

- Batchelor, G.K. (1959). Small-scale variation of convected quantities like temperature in turbulent fluid, *J. Fluid Mech.*, Vol. 5, 113-133.
- Chaouat, B., Schiestel, R. (2005). A new partially integrated transport model for subgrid-scale stresses and dissipation rate for turbulent developing flows, *Phys. Fluids*, Vol. 17, 065106, 1-19.
- Chaouat, B. (2011). An efficient numerical method for RANS/LES turbulent simulations using subfilter scale stress transport equations. *Int. J. Numer. Methods Fluids*, Vol. 67, 1207-1233.
- Chaouat, B. (2017). The state of the art of hybrid RANS/LES modeling for the simulation of turbulent flows. *Flow, Turbul. Combust.*, Vol. 99, 279-327.
- Hanjalic, K., Launder, B.E. (2011). *Modelling turbulence in engineering and the environment. Second-moment route to closure*, Cambridge University Press.
- Kasagi, N., Kuroda, A., Hirata, M. (1989). Numerical investigation of near-wall turbulent heat transfer taking into account the unsteady heat conduction in the solid wall, *Int. J. Heat Mass Transfer*, Vol. 111, 385-392.
- Kawamura, H., Ohsaka, K., Abe, H., Yamamoto, K. (1998). DNS of turbulent heat transfer in channel flow with low to medium-high Prandtl number fluid, *Int. J. Heat Fluid Flow*, Vol. 19, 482-491.
- Kawamura, H., Abe, H., Matsuo, Y. (1999). DNS of turbulent heat transfer in channel flow with respect to Reynolds and Prandtl number effects, *Int. J. Heat Fluid Flow*, Vol. 20, 196-207.
- Kenjeres, S., Hanjalic, K. (2006). LES, T-RANS and hybrid simulations of thermal convection at high  $Ra$  numbers, *Int. J. Heat Fluid Flow*, Vol. 27, 800-810.
- Kozuka, M., Seki, Y., Kawamura, H. (2009). DNS of turbulent heat transfer in a channel flow with a high spatial resolution, *Int. J. Heat Fluid Flow*, Vol. 30, 514-524.
- Lu, D.M, Hetsroni, G. (1995). Direct numerical simulation of a turbulent open channel flow with passive heat transfer, *Int. J. Heat Mass Transfer*, Vol. 38, (17), 3241-3251.
- Lyons, S.L., Hanratty, T.J., McLaughlin, J.B. (1991). Direct numerical simulation of passive heat transfer in a turbulent channel flow, *Int. J. Heat Mass Transfer*, Vol. 34, 1149-1160.
- Matsubara, K., Sakurai, A., Miura, T., Kawabata, T. (2012). Spanwise heat transport in turbulent channel flow with Prandtl numbers ranging from 0.025 to 5.0, *J. Heat Transfer*, Vol. 134, 1-7.
- Mosyak, A., Pogrebnyak, E., Hetsroni, G. (2001). Effect of constant heat flux boundary condition on wall temperature fluctuations, *J. Heat Transfer*, Vol. 123, 213-218.
- Tennekes, H., Lumley, J.L. (1972). *A First Course in Turbulence*, the MIT Press.